Computerized Medical Imaging and Graphics 34 (2010) 213–227

Contents lists available at ScienceDirect

Computerized Medical Imaging and Graphics

journal homepage: www.elsevier.com/locate/compmedimag

Multi-scale retinal vessel segmentation using line tracking

Marios Vlachos*, Evangelos Dermatas

Department of Electrical Engineering and Computer Technology, University of Patras, Patras, Greece

ARTICLE INFO

Article history:
Received 1 June 2009
Received in revised form
24 September 2009
Accepted 25 September 2009

Keywords:
Multi-scale line tracking
Cross-sectional profile
Morphological reconstruction
Retinal images
Vessel segmentation

ABSTRACT

In this paper an algorithm for vessel segmentation and network extraction in retinal images is proposed. A new multi-scale line-tracking procedure is starting from a small group of pixels, derived from a brightness selection rule, and terminates when a cross-sectional profile condition becomes invalid. The multi-scale image map is derived after combining the individual image maps along scales, containing the pixels confidence to belong in a vessel. The initial vessel network is derived after map quantization of the multi-scale confidence matrix. Median filtering is applied in the initial vessel network, restoring disconnected vessel lines and eliminating noisy lines. Finally, post-processing removes erroneous areas using directional attributes of vessels and morphological reconstruction.

The experimental evaluation in the publicly available *DRIVE* database shows accurate extraction of vessels network. The average accuracy of 0.929 with 0.747 sensitivity and 0.955 specificity is very close to the manual segmentation rates obtained by the second observer. The proposed algorithm is compared also with widely used supervised and unsupervised methods and evaluated in noisy conditions, giving higher average sensitivity rate in the same range of specificity and accuracy, and showing robustness in the presence of additive Salt&Pepper or Gaussian white noise.

1. Introduction

The retina, a layer of membrane at the back of the eye, can be visualized as an image by the fundus camera. The retinal images, often noisy, poorly contrasted and non-uniformly illuminated suffer from brightness variations both along the same image and between different images.

Several supervised [1–3] and unsupervised [4–6] vessel segmentation methods have already been proposed and evaluated. Valuable applications has been presented [7,8] in the diagnosis of various eye and systemic diseases, such as diabetes, hypertension [9], and angiogenesis [10]. The most accurate supervised methods enhance their detection capabilities using several types of knowledge about the vessel network morphology.

An automated vessel location method in ocular fundus images is proposed using a novel cooperative synergy of local and global features to segment the vessel network [11]. Such a tool should be proved useful to eye care specialists for purposes of patient screening, treatment evaluation, and clinical studies. A method for rapid, automatic, robust, adaptive, and accurate tracing of retinal vasculature and analysis of intersections and crossovers is presented in [12] and is being applied to computer-assisted laser retinal surgery.

In a typical vessel segmentation method, after the initial estimation of a vessel network, fine tuning methods are used to improve the detection accuracy. In unsupervised segmentation, the vessel network is detected using pixel-based processing methods through spatial transformations or tracking operations. The tree-like geometry of the vessel network makes it a usable feature for registration between objects of a different nature. Vessel-like patterns are detected with respect to precise models. If a vessel is defined as a bright pattern, piece-wise connected and locally linear mathematical morphology operators are used to produce this type of description. In order to discriminate vessels from similar background patterns, a cross-curvature evaluation is performed. The vessels are separated out as they have a specific Gaussian-like profile whose curvature varies smoothly along the vessel.

The most popular pixel based segmentation methods include, two-dimensional matched filters [4,10], object classification and noise removal [13], continuous two-dimensional Morlet wavelet transformation at multiple scales [2], allowing noise filtering and vessel enhancement in a single step [1]. In [14], curvature evaluation is used to detect vessel-like patterns in a noisy environment. Computational models reduce noise and enhance the vessels network combining Naka-Rushton, cluster, hyperbole, median filters and skeleton processes. As a result, bifurcations and crossover pixels of retinal vessels are detected [15].

Several vessel detection algorithms are based on a four steps procedure: noise reduction, Gaussian-like profile enhancement,

* Corresponding author. Tel.: +30 2610996189.
E-mail address: mvlachos@george.wcl2.ee.upatras.gr (M. Vlachos).

0895-6111/$ – see front matter © 2009 Elsevier Ltd. All rights reserved.
doi:10.1016/j.compmedimag.2009.09.006

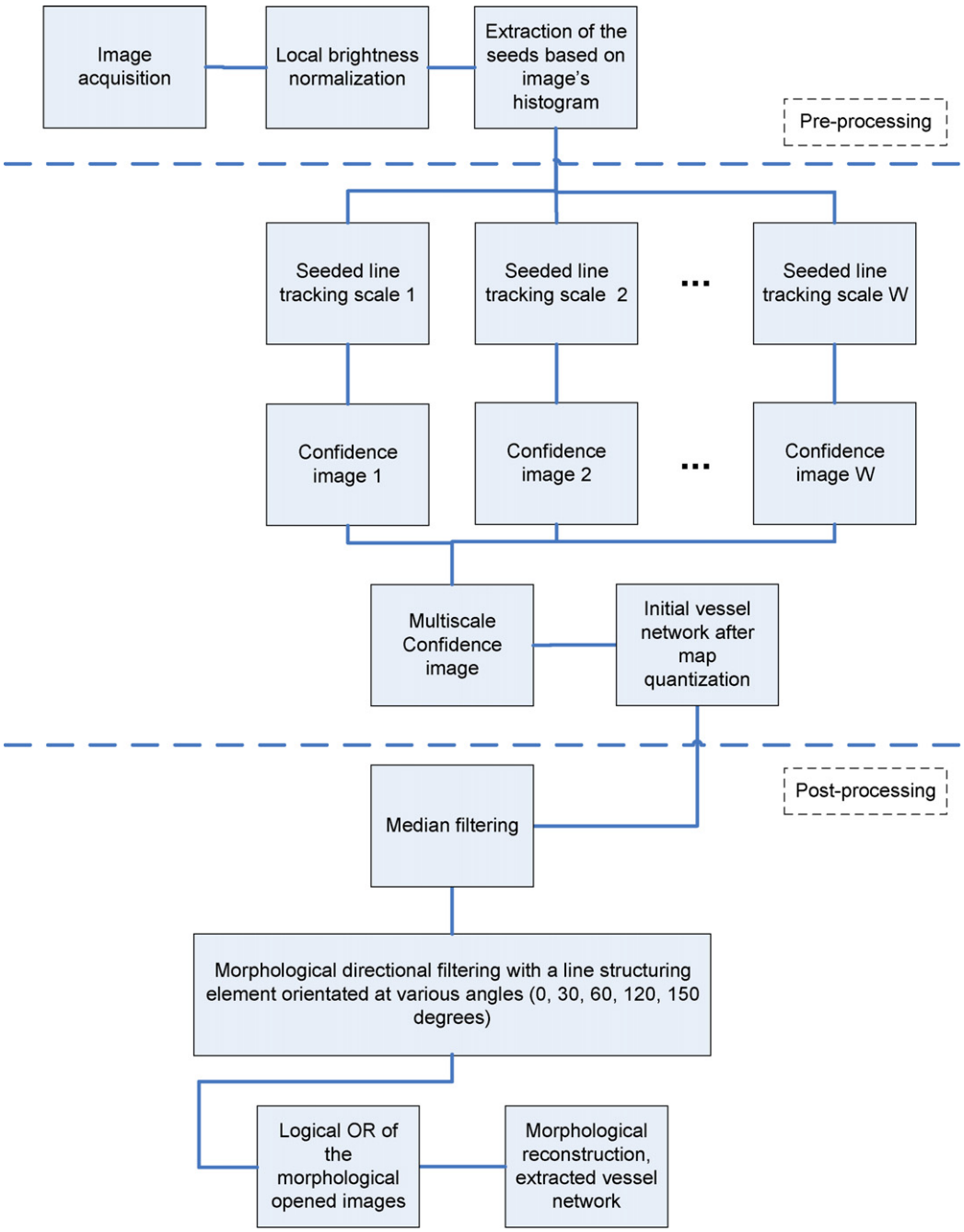

Fig. 1. Flowchart of the seeded multi-scale line-tracking algorithm (*MSLTA*).

cross-curvature evaluation and linear filtering. Based on the analysis of gradient orientation, where circular and linear structures are detected, a robust and efficient method for detection of anatomical features is used in low contrast and non-uniformly illuminated retinal images [9]. A multi-scale approach is employed to detect various sizes of features, especially blood vessels with varying diameters.

A second-order derivative Gaussian matched filter is used to locate the center point and width of a vessel in its cross-sectional profile [5]. In addition, the extended Kalman filter is employed for the optimal linear estimation of the next possible location of blood vessel segment and a simple branching detection strategy is implemented checking the bifurcation in the vessel network during tracking. In a similar approach, the fitness of estimating vessel profiles with Gaussian function is evaluated and an amplitude-modified second-order Gaussian filter is proposed for the detection and measurement of vessels [16].

Even in case of robust vessel segmentation, post-processing methods are used to remove false detected vessels, improving further the detection accuracy. The most important methods include mathematical morphology transformation [1], length filtering and vascular intersection detection [6], vessel detection based on piecewise linearity and anti-parallel edges [17] or detection of morphological similarities between image ridges and vessel centerlines [3]. The ridges are used to partition the original image into patches by composing primitives in the form of line elements. Each image pixel is assigned to the closest line element using a feature vector and the nearest neighbor classifier [3]. In angiograms, branching and bifurcation regions of typical vessel trees are detected decreas-

ing significantly the false positive rate in the segmented vessel network [18].

Recently, a new technique extracts vessels in retinal images, improving the detection rate of low-contrast and narrow vessels, decreasing also the false detections at non-vascular structures [19]. The core of this technique is a new likelihood ratio test that combines matched-filter responses at different widths, confidence measures defined as a vector projection of the normalized brightness at each pixel neighborhood onto a vessel profile and vessel boundary measures. At each pixel, these responses form a six-dimensional vector. A training technique is used to develop a mapping of this vector to a likelihood ratio that measures the pixel—"vesselness". The new vesselness likelihood ratio is embedded into a vessel tracing framework, resulting in an efficient and effective vessel centerline extraction algorithm.

A method for personal identification based on finger-vein patterns is presented and evaluated in [20,21], using an iterative line tracking starting at various positions. Taking into account the excellent line-tracking results [20,21], an improvement of the finger vein pattern extraction method has been proposed for the case of retinal vessel segmentation [22]. The most important limitations in [20,21] are related to its stochastic nature that results in a different vessel network for every execution, and the large number of manually tunable parameters. Apart from these limitations the algorithm must be adapted in order to be able to detect vessels of various diameters. Thus, our work is focused on how to tackle the problems of [20,21] with subsequent goal the fully automatic and robust segmentation of the retinal vasculature in case of noisy images.

In this paper, a novel algorithm for vessels network extraction is presented and evaluated using a fast deterministic multi-scale vessels network extraction method for efficient segmentation of retinal vasculature under adverse conditions. The multi-scale analysis facilitates the vessel detection at different diameters avoiding also the detection of noisy vessel-like structures, brightness variations and noise.

The remaining of this paper is organized as follows. In Section 2, the multi-scale single channel line-tracking algorithm (*MSLTA*) is presented, followed by a comparison with the iterative line-tracking algorithm (*ILTA*). The experimental evaluation of the two algorithms is presented and discussed in Section 4. In the same section the proposed algorithm is also compared with the most widely used algorithms in the field of retinal vessel segmentation and is evaluated under noise presence. Finally, some conclusions are given.

2. Multi-scale single channel line-tracking algorithm

A flowchart of the retinal vessel segmentation algorithm is given in Fig. 1. Several image processing modules are employed: local normalization of brightness compensates luminosity and contrast variability, seeds extraction derives the most appropriate pixels as vessel candidates and line tracking starting from the extracted seeds and repeating for a number of scales is used to estimate for each pixel a multi-scale confidence to belong to a vessel. Consequently, map quantization and median filtering disconnect noisy lines, bridge gaps increasing the accuracy of the confidence array. Finally, morphological post-processing removes the remaining outliers.

The vessels network is extracted by processing a single color channel, a gray-scale digital image or any single channel estimated from a linear or non-linear transformation of a multi-channel image. In this paper the retinal images of the publicly available *DRIVE* database [23] were used to evaluate the proposed algorithm. In Figs. 2 and 5–7, the corresponding image at each processing step for the green channel of the first *RGB* retinal image (01_test.tif, Fig. 2) is shown. The green channel is used because it presents the highest contrast between regions belonging to the vessels' network and the background.

Fig. 2. Green channel of the first image of the *DRIVE* database.

Step 1. Initialization

Retinal images usually suffer from large variability in contrast and luminosity both between different images and along the same image, impeding the development of automatic algorithms. Therefore, an efficient local normalization of brightness method is applied [24]. This method is based on the estimation of the luminosity and contrast variability in the background part of the image and the subsequent compensation of this variability in the whole image.

Step 2. Selection of starting pixels (seeds) for line tracking

If $I(x, y)$ denote the pixel brightness of the normalized image at position (x, y), a set of seed pixels V_s containing the initial pixels from which the *MSLTA* start seeking for a vessel path, is defined

$$V_s = \{(x, y) : T_{LOW} < I(x, y) < T_{HIGH}\}, \quad (1)$$

where T_{LOW} and T_{HIGH} are the two thresholds automatically estimated from the histogram using the size of the expected vessel area, as shown in Fig. 3. The threshold T_{LOW} is estimated by the percentile of pixels that hold high confidence to belong to the dark background, while the threshold T_{HIGH} is estimated by the percentile of dark background and vessel pixels. In the *DRIVE* database the corresponding percentile coverage are approximately 30 and 70%. The remaining bright background holds pixels with high confidence to belong to the bright tissue such as optic disk and bright lesions. These rates are statistically estimated using the provided manual segmentation which separates vessel from background pixels and the provided mask which separates the dark background from the vessels-surrounding tissue. The variance of the statistical estimations is very low between images in the *DRIVE* database.

The number of seed pixels affect the robustness of the confidence array. If, an extremely small group of seeds is selected from a very narrow histogram area, the detection accuracy of the algorithm is decreased because some vessel lines cannot be reached

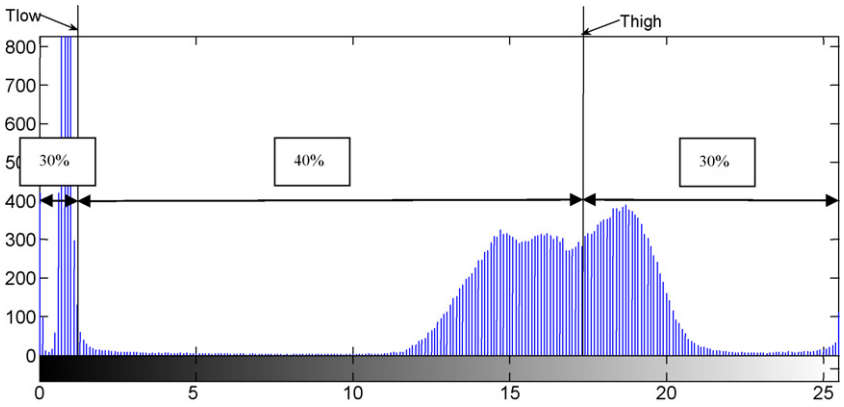

Fig. 3. The histogram of the green channel of the first image of the *DRIVE* database and the thresholds T_{LOW} and T_{HIGH}.

from the available seeds. On the contrary, the selection of a large number of seeds, achieved from a wide histogram area, increases both fault positive rate and computational time. So, special care must be taken in order to ensure that the selected group of seeds is representative and the computational complexity remains in acceptable levels. The seeds extraction process is not crucial for the accuracy of the proposed algorithm because the post-processing steps are able to tackle small increments in the fault positive rate.

During the line-tracking process, the confidence of each pixel to belong to a vessel line at an odd scale W, is estimated and stored in the array C_W. A large entry in the confidence array represents high confidence that the corresponding pixel belong to the vessel network. Initially, all the elements of the confidence array and for all scales are set to zero:

$$C_W(x, y) := 0. \tag{2}$$

The steps 3 and 4 are executed T_s times ($t = 1{:}T_s$) where T_s = length (V_s) for all pixels belong in the set of seeds V_s and for all scales W.

Step 3. Initialization of line tracking

$k := 1$, $V_c(k) := V_s(t)$, $C_c := \{\}$, where V_c is the set of pixels tracked in the current iteration t and C_c is the set of new line-tracking pixels.

Step 4. Estimation of the new line-tracking pixel

The coordinates of the current tracking pixel are the last entry of V_c. The set of the candidate pixels, denoted as C_c, are the eight nearest neighbors N_8 of the current tracking pixel, excluding the pixels included in V_c:

$$C_c = N_8(V_c(k)) - V_c. \tag{3}$$

For all the candidate pixels included in the C_c, the cross-sectional profile parameter V_l is estimated as:

$$\begin{aligned} &V_l((x, y), (r, \vartheta_i)) = I(x + \lfloor r\ \cos\vartheta_i - w\ \sin\vartheta_i \rfloor\ , \\ &y + \lfloor r\ \sin\vartheta_i + w\ \cos\vartheta_i \rfloor) + I(x + \lfloor r\ \cos\vartheta_i + w\ \sin\vartheta_i \rfloor\ , \\ &y + \lfloor r\ \sin\vartheta_i - w\ \cos\vartheta_i \rfloor) - 2I(x + \lfloor r\ \cos\vartheta_i \rfloor\ , \\ &y + \lfloor r\ \sin\vartheta_i \rfloor), \quad (x, y) \in C_c \ \text{ and } \ w = \frac{W-1}{2}, \end{aligned} \tag{4}$$

where (r, θ_i) are the polar coordinates of the candidate relative to pixel (x, y) and W is the width of the cross-sectional profile. In case where the value of parameter r is set to unity, the cross-sectional profile parameter can be approximated using the computational efficient equation:

$$V_l((x, y)) = \begin{cases} I(x \pm 1, y + w) + I(x \pm 1, y - w) - 2I(x \pm 1, y) \\ I(x + w, y \pm 1) + I(x - w, y \pm 1) - 2I(x, y \pm 1) \\ I(x \pm 1 + w, y \pm 1 - w) + I(x \pm 1 - w, y \pm 1 + w) - 2I(x \pm 1, y \pm 1) \\ I(x \pm 1 + w, y \mp 1 + w) + I(x \pm 1 - w, y \mp 1 - w) - 2I(x \pm 1, y \mp 1) \end{cases}, \quad (x, y) \in C_c. \tag{5}$$

In Fig. 4 the estimation of parameter V_l is shown. *Curtrac* is the current tracking pixel, *bac1* is the background pixel located $W/2$ pixels away from *cand*, *bac2* is the background pixel located $W/2$ pixels away from *cand* but in the opposite direction. *Cand* is the candidate pixel included in the set C_c. As shown in Fig. 4a, if the

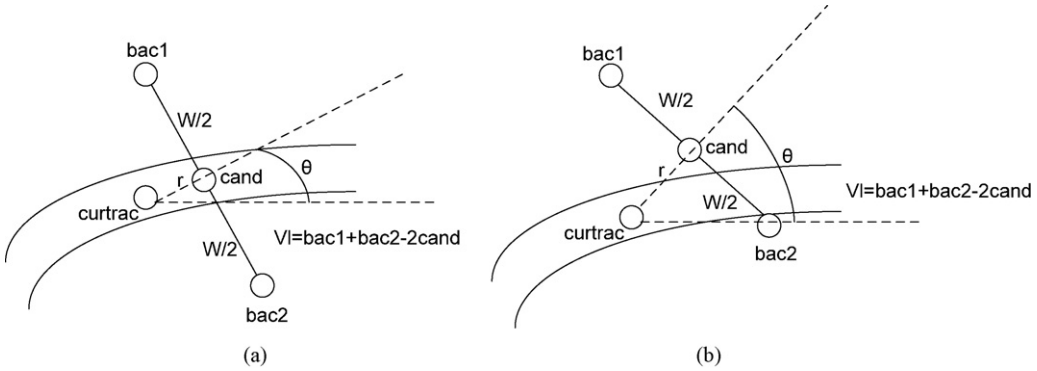

Fig. 4. Estimation of the cross-sectional parameter V_l. (a) The candidate pixel (*cand*) belongs to the vessel network, (b) the candidate pixel (*cand*) do not belong to the vessel network.

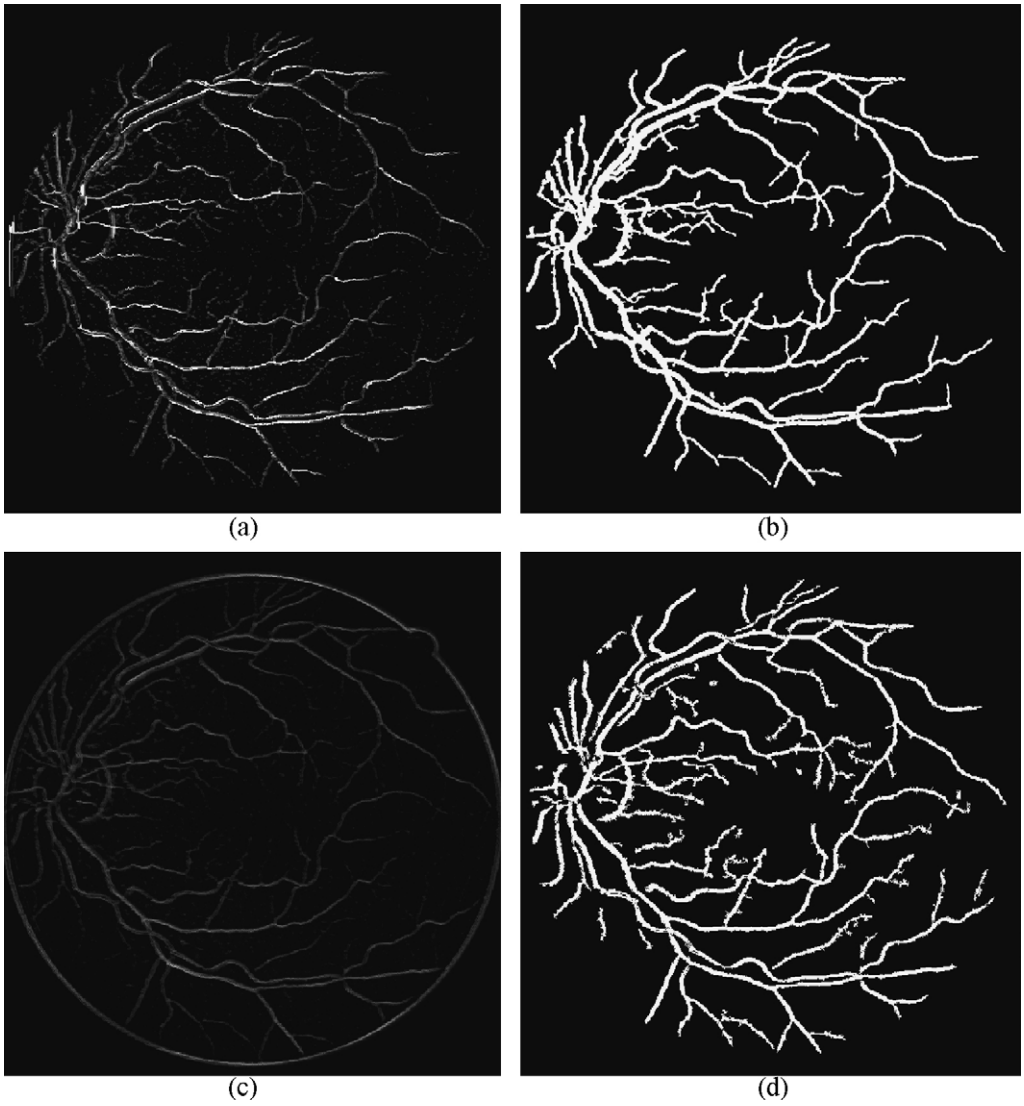

Fig. 5. *MSLTA*. (a) Multi-scale confidence array, (b) vessel map after morphological post-processing, *ILTA*, (c) confidence array and (d) vessel map after morphological post-processing.

candidate pixel belongs to the vessel network, the cross-sectional parameter V_l has a large positive value. On the other hand, if the candidate pixel belongs to background (Fig. 4b), the brightness of pixels *bac1*, *bac2* and *cand* have similar values and thus the parameter V_l has value near to zero.

The angle with the maximum positive cross-sectional profile parameter, exceeding also a predefined threshold T:

$$\vartheta_o = arg \max_{\vartheta_i} \{V_l((x,y),(r,\vartheta_i)) : V_l((x,y),(r,\vartheta_i)) > T\}, \quad (6)$$

is used to define the new current tracking pixel:

$$(x_c, y_c) = (x + r\ \cos\vartheta_o, y + r\ \sin\vartheta_o). \quad (7)$$

In Section 4 an appropriate value for the threshold T is derived.

The current tracking pixel is added to V_c:

$$k{:=}k+1, \quad V_c(k){:=}(x,y). \quad (8)$$

Then, the confidence array C_W is updated:

$$C_W(x,y){:=}C_W(x,y)+1, \quad (x,y){:=}(x_c,y_c), \quad (9)$$

and the searching procedure for a new tracking pixel is repeated from step 4.

If all cross-sectional profile parameters in Eq. (6) are less than threshold T, the line-tracking algorithm is started for the next seed pixel ($t{:}=t+1$) from step 3.

The study of the cross-sectional profiles and the corresponding cross-sectional positions in the original image show that the pixel with minimum brightness in the cross-sectional profile belongs to a vessel line (Fig. 1), i.e. the value of V_l reflects the curvature of the cross-section. The simple and effective method of pixels elimination using the positive threshold T is used to reduce fault line tracking in noisy images, an improvement on the *ILTA* [20,21].

Step 5. Multi-scale line tracking

The *MSLTA* for all seed points is repeated for a fixed number of scales. The number of scales is selected in accordance to the size of the diameter of the tubular structures that have to be detected in the retinal image. A large number of scales is required in case of high variance of the vessels diameters in the retinal images. In the retinal images of *DRIVE* database, a number of five scales $W=3$, 5, 7, 9 and 11 proved adequate.

In applications where the detection of vessel networks at specific widths is critical, the total confidence array is estimated from the weighted sum of the individual estimations at different

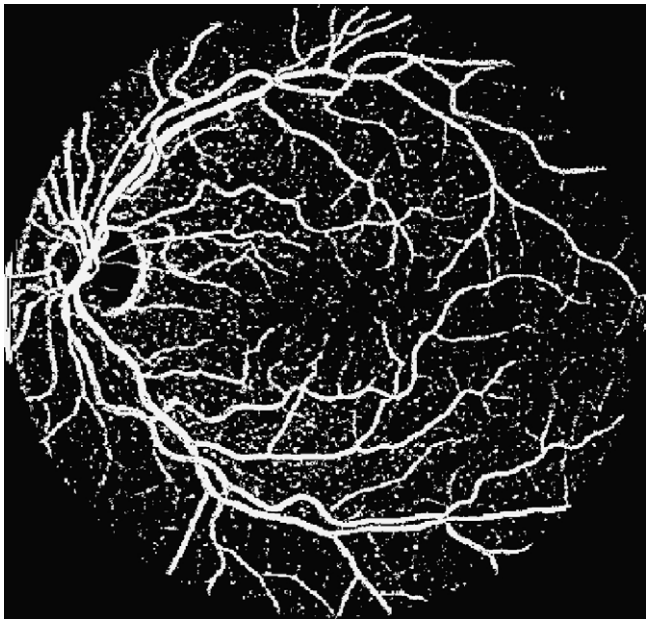

Fig. 6. Initial vessel map using map quantization.

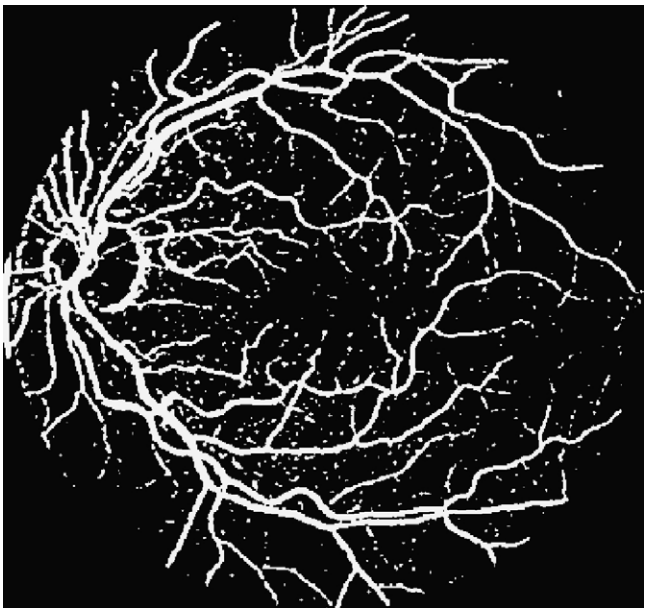

Fig. 7. Vessel map after median filtering.

scales. In such case the weights are defined according to the width preference, i.e. larger values are preferred for the widths to be detected and smaller for the remaining. Otherwise, the multi-scale confidence array is derived by summing up the confidence arrays, as shown in Fig. 5a.

Step 6. Initial estimation of vessel network

The initial estimation of the vessel network is derived using a fast and simple selection process named map quantization, instead of the well-known local neighboring thresholding method [22]. The initial vessel network is constructed from the pixels with confidence matrix value greater than a threshold T_c, with typical value equal to the number of scales. Pixels that have in the confidence matrix value greater than the number of scales should belong to vessel network. Due to noise, and very rarely, some non-vessel pixels can be tracked in all scales and erroneously be considered as part of the vessel network. Consequently, the adopted selection process reduces the presence of noisy pixels in the vessel network. In Fig. 6, the initial vessel map obtained using map quantization is shown.

Step 7. Median filtering of the initial vessel network

The median filtering is used to re-establish the connection (bridge gaps) of several vessel lines, to reveal some hidden pixels that belong to vessel lines and simultaneously to decrease the false detection rate by removing part of the remaining noisy pixels. As shown in Fig. 7, the segmentation accuracy of the vessel network is improved, when a 3×3 median filter is applied to the initial vessel map.

Step 8. Morphological directional filtering

This step is essential because after median filtering several misclassifications have still remained (Fig. 7). The binary image is transformed using five different morphological openings with line structuring elements orientated in five different directions 0°, 30°, 60°, 120° and 150° [25]. In the line structuring elements, a length of M pixels is adopted, to preserve only vessel like structures with length equal or larger than M. The output image of this process is derived using the logical *OR* of the five responses.

Step 9. Vessel network using morphological reconstruction

In the final step, a process called morphological reconstruction is applied to eliminate few erroneous regions such as small blobs, producing the final vessels network. This transformation process involves two images and a structuring element. The first image is the marker and contains the transformation's starting point. The second image is the mask and contains the constraint rules. The structuring element that used defines connectivity.

The fast hybrid reconstruction algorithm, described in [26], is implemented using as mask image the output of the directional filtering and as a marker, the morphological opening of the directional filtering output. The structuring element eliminates all remaining isolated misclassified regions that have radius smaller than R pixels. Fig. 5b shows the final reconstructed image, which is the desirable vessel map. The whole *MSLTA* is summarized in the form of pseudocode in Fig. 8.

A small number of parameters (r, W, T, M, R) is used to adapt the algorithm behavior in different vessel segmentation applications and imaging systems. The expected width of the cross-sectional profile W is restricted by the minimum and maximum diameter of the tubular vessels structure to be detected. In different applications, tubular structures similar to vessels i.e. leaf veins, roads in satellite imagery can also be detected by the proposed algorithm. These structures usually have smaller or higher brightness than the background with the cross-section profile looks like valley or ridge respectively.

The distance r between the current tracking pixel and the testing neighborhood is set in our application to one (immediate neighborhood), due to tiny differences in the segmentation accuracy of the algorithm when distances less than 10 are used. The threshold T is the maximum expected curvature of a vessel cross-sectional profile. This parameter is closely related to the presence of blurring, due to scattering or scene moving effects, and the contrast level of the image.

The presence of the outliers in the initial segmentation result, a typical image is shown in Fig. 6, depends strongly on the threshold value involved in the quantization process. Therefore, if a hard threshold is used to obtain the binary vessel map, a smaller number of outliers would distort the estimated vessel network. On the contrary, when a soft threshold is used a larger number of out-

```
OrgIm=ImageAcquisition()
PreIm=Preprocessing(OrgIm)
Vs=SeedExtraction(PreIm)
for W=InitScale:Wstep:FinScale
    for t=1:length(Vs)
        V_C={}
        C_C={}
        k=1
        V_C(k)=V_S(t)
        while(Vlmax>T)
            C_C=N_θ(V_C(k))-V_C
            θ_0= arg max_{θ_i} {Vl((x,y),(r,θ_1)): Vl((x,y),(r,θ_1))>T}
            k=k+1
            V_C(k)=(x,y)
            C_W(x,y)=C_W(x,y)+1
            (x,y)=(x+rcosθ_0,y+rsinθ_0)
        end
    end
end

C=sum(C_W)
for i=1:Crows
      for j=1:Ccolumns
            if(C(i,j)>=Nscales)
                  Bw(i,j)=1
            else
                  Bw(i,j)=0
            end
  end
end
Bw2=MedianFiltering(Bw)
Bw3=MorphologicalPostprocessing(Bw2)
```

Fig. 8. Pseudocode of the *MSLTA*.

liers would survive such as circular blobs and shapeless structures. In morphological post-processing, the length of the line structuring element M, and the radius R of the disk structuring element are closely related to the length of the smallest line segment and the radius of the smallest blob that would be retained after image cleaning. Morphological directional filtering eliminates shapeless structures disconnected from the main vessel network while morphological reconstruction eliminates also disconnected circular blobs.

The proposed *MSLTA* can be extended in case of multi-channel images as *ILTA* [22]. In this case independent color channel recordings of the vessel map are available. Applying the proposed algorithm for each available channel, multiple estimations of vessel network are derived. The final vessel map is estimated using the logical *OR* of the channel-independent estimations.

3. Multi-scale versus iterative line tracking

Theoretical comparison between different detectors of vessel maps is difficult to be obtained, due to significant differences between the implemented algorithms and the close relation between the algorithms computational complexity and the scene context. Therefore in this section, the *MSLTA*, the popular *ILTA* and its variants [20–22] are studied comparing the adopted algorithmic solutions.

The major disadvantages of the *ILTA* for retinal vessel segmentation [22] are its stochastic nature, estimating a different vessel network every time the algorithm is executed, the large number of the manually defined stochastic parameters and the hypothesis of the fixed vessels diameter. The last hypothesis is the most important source of vessel detection errors with diameter different than the specified.

In the proposed algorithm the first problem regarding the stochastic nature of the *ILTA* is solved by using a non-iterative seeded line-tracking module. In this case the line-tracking algorithm starts from a set of seeds using the expected coverage of the vessel network. A simple and computational efficient rule identifies the pixels with brightness within two thresholds that hold high confidence to belong to the vessel's network. This rule is based on the observation that vessel pixels have greater brightness than the dark background and lower brightness than other parts of the retina. The thresholds T_{LOW}, and T_{HIGH} are estimated using the dark background coverage which is almost the 30% of the image size in the *DRIVE* database, the vessels network, covering the 40%, and the remaining bright background. As already mentioned, the seeds selection process used in line-tracking initialization affects significantly the computational time. However, it is not crucial for the segmentation accuracy of the *MSLTA*.

The second problem regarding the *ILTA* is the usage of a large set of tunable parameters. These parameters are used to select the 8-pixel neighborhood or various 3-pixel directional neighborhood in an attempt to segment directed veins in infrared images of fingers [20,21]. In retinal images this is not the case. Vessels are originated from the optic disk and follow excessive trajectories with a lot of bifurcations and junctions, thus directional preferences are useless.

In the *ILTA* implementation [22], the initial estimation of vessels network is derived by local thresholding of the confidence array with a threshold image $T(x, y)$. In the proposed *MSLTA*, instead of using this thresholding technique, a map quantization technique is adopted. In the evaluation experiments significant differences between *ILTA* and *MSLTA* are encountered when different modules are implemented. Therefore, the most effective module for both algorithms is selected by comparing the average segmentation accuracy in the *DRIVE* database. In *ILTA*, the local neighboring thresholding gives the greater segmentation accuracy. On the contrary, in the *MSLTA* implementation, the best accuracy is achieved using map quantization. The adopted map quantization process increases the true vessel detection rate, as shown in the experimental evaluation. False vessel detection is successfully tackled during post-processing.

In the *MSLTA*, the maximum expected curvature T is used to accept only sufficient large cross-sectional profiles. This threshold employed because some profiles are quite noisy giving positive V_l value for the testing pixel without this pixel truly belong to the vessel network, as met in [20,21].

The *MSLTA* is performed for a number of different scales, instead of the single scale proposed in [22], and the estimated confidence matrices are combined in the intermediate multi-scale image map. Thus, the proposed algorithm can be used to detect tubular dark or bright structures in various image processing and image analysis problems. The width W of the testing cross-sectional profile is used in both algorithms. In the *ILTA* a single experimentally derived value is used. In the *MSLTA* a wide range of values are defined, detecting tubular structures of different diameters. In this sense, the disadvantage of the manually defined parameter was significantly reduced by using a wide range of values.

The computational complexity of the proposed algorithm is significantly affected by the number of the seeds that must be tracked. Minor variations in the computational complexity are met using different images and the same thresholds T_{LOW} and T_{HIGH}, while in the *ILTA* the computational complexity depends on the iterations number. In order to achieve reliable results, the number of *ILTA* iterations and thus the computational time must be increased enormously. Consequently, for robust retinal vessel segmentation the *MSLTA* outperforms the *ILTA* because it adequately segments the vasculature in a significantly smaller number of tracking steps.

In both algorithms a significant part of the optic disk is included in the vessels network, because no special care has been taken to prevent this type of segmentation error. A dedicated variant of both algorithms can be used to decrease the false positive rate in retinal images, as proposed in [27].

Table 1
Sensitivity, specificity and accuracy of the *MSLTA* using the two different V_1 estimators (Eqs. (4) and (5)) at successive processing modules in the *DRIVE* database.

	Sensitivity		Specificity		Accuracy	
	Average	Standard deviation	Average	Standard deviation	Average	Standard deviation
MSLTA using Eq. (4)						
Map quantization	**0.7964**	0.0543	**0.8871**	0.0249	**0.8755**	0.0191
Median filtering	**0.8013**	0.0582	**0.9201**	0.0222	**0.9049**	0.0172
Morphological filtering	**0.7616**	0.0630	**0.9522**	0.0133	**0.9279**	0.0096
Morphological reconstruction	**0.7468**	0.0655	**0.9551**	0.0128	**0.9285**	0.0088
Length filtering	**0.7602**	0.0627	**0.9490**	0.0145	**0.9249**	0.0105
MSLTA using Eq. (5)						
Map quantization	**0.8254**	0.0482	**0.8625**	0.0367	**0.8649**	0.0220
Median filtering	**0.8189**	0.0527	**0.9071**	0.0256	**0.8957**	0.0199
Morphological filtering	**0.7805**	0.0572	**0.9467**	0.0156	**0.9254**	0.0118
Morphological reconstruction	**0.7670**	0.0601	**0.9498**	0.0148	**0.9263**	0.0108
Length filtering	**0.7830**	0.0569	**0.9424**	0.0172	**0.9219**	0.0129

4. Experimental results

The proposed algorithm is evaluated using the retinal images of the *DRIVE* database [28], containing both healthy and humans suffer from diabetic retinopathy. The screening population consists of 400 diabetic subjects between 25 and 90 years of age. Forty images have been randomly selected, 33 do not show any sign of diabetic retinopathy and seven show signs of mild early diabetic retinopathy. Each image was acquired using 8 bits accuracy per color at 768×584 pixels. The set of 40 images has been divided into two disjoint sets, training and testing, both containing 20 images. For the training images, single manual segmentation data of the vasculature network are available. Two manual segmentations are available for the test cases; one is used as gold standard, the other one can be used to compare computer generated segmentations with those of an independent human observer. In this study, the green channel of the *RGB* retinal images is used for single channel vessel network extraction, because this channel has the highest contrast between regions belong to the vessels' network and the background [11].

In the retinal vessel segmentation process, the outcome is a pixel-based classification result. Any pixel is classified either as vessel or surround tissue. Consequently, there are four events, true positive (TP) and true negative (TN) when a pixel is correctly segmented as a vessel or non-vessel, and two misclassifications, a false negative (FN) appears when a pixel in a vessel is segmented in the non-vessel area, and a false positive (FP) when a non-vessel pixel is segmented as a vessel-pixel.

Two widely known statistical measures are used for algorithm evaluation: sensitivity and specificity, of the binary segmentation outcome. The sensitivity is a normalized measure of true positives, while specificity measures the proportion of true negatives

$$\text{sensitivity} = \frac{\text{TP}}{\text{TP}+\text{FN}} \quad \text{and} \quad \text{specificity} = \frac{\text{TN}}{\text{TN}+\text{FP}}.$$

The tradeoff between the two measures is graphically represented with the receiver operating characteristic curve (ROC), which is a plot of the sensitivity versus 1 – specificity. Equivalently, ROC curve can be represented by plotting the true positive rate (TPR) versus the false positive rate (FPR). These rates are the fractions of TPs and FPs:

$$\text{TPR} = \frac{\text{TP}}{\text{TP}+\text{FN}} = \text{sensitivity},$$

$$\text{FPR} = \frac{\text{FP}}{\text{FP}+\text{TN}} = 1 - \frac{\text{TN}}{\text{TN}+\text{FP}} = 1 - \text{specificity}.$$

The accuracy of the binary classification is defined by

$$\text{accuracy} = \frac{\text{TP}+\text{TN}}{P+N},$$

where P and N represent the total number of positives (vessel) and negatives (non-vessel) pixels in the segmentation process. The accuracy is the degree of conformity of the estimated binary classification to the ground truth according to a manual segmentation. Thus, the accuracy is strongly related to the segmentation quality and for this reason is used to evaluate and compare different methods.

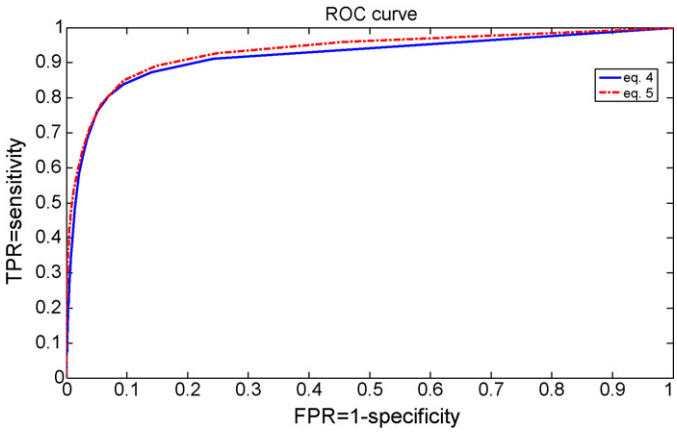

Fig. 9. ROC curves of two different *MSLTA* implementations using Eqs. (4) and (5) and different values of threshold T_c.

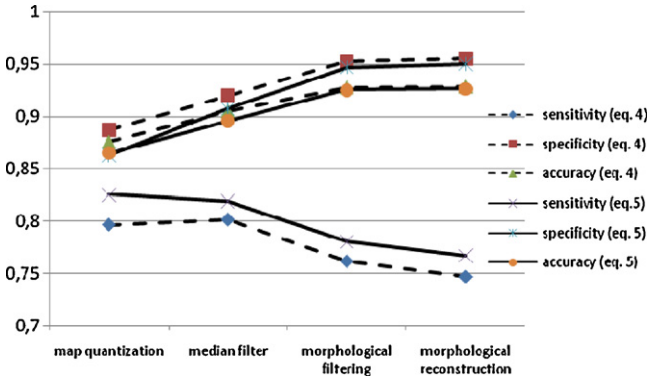

Fig. 10. Sensitivity, specificity and accuracy of the *MSLTA* using Eqs. (4) and (5) after map quantization, median filtering, morphological filtering and morphological reconstruction.

Table 2
Mean sensitivity, specificity, and accuracy for the testing set of the *DRIVE* database using different vessel segmentation methods.

	Sensitivity		Specificity		Accuracy	
	Average	Standard deviation	Average	Standard deviation	Average	Standard deviation
Human observer	**0.7761**	0.0593	**0.9725**	0.0082	**0.9473**	0.0048
Supervised methods						
Niemeijer	**0.6793**	0.0698	**0.9801**	0.0085	**0.9416**	0.0064
Staal	**0.7193**	0.0694	**0.9773**	0.0087	**0.9441**	0.0057
Unsupervised methods						
Chaudhuri	**0.2716**	0.2118	**0.9794**	0.0388	**0.8894**	0.0231
Jiang	**0.6478**	0.0642	**0.9625**	0.0129	**0.9222**	0.0069
Zana	**0.6696**	0.0764	**0.9769**	0.0079	**0.9377**	0.0077
Perez	**0.7086**	0.1815	**0.9496**	0.0260	**0.9181**	0.0239
ILTA	**0.6960**	0.0451	**0.9416**	0.0136	**0.9100**	0.0111
MSLTA	**0.7468**	0.0654	**0.9551**	0.0128	**0.9285**	0.0088

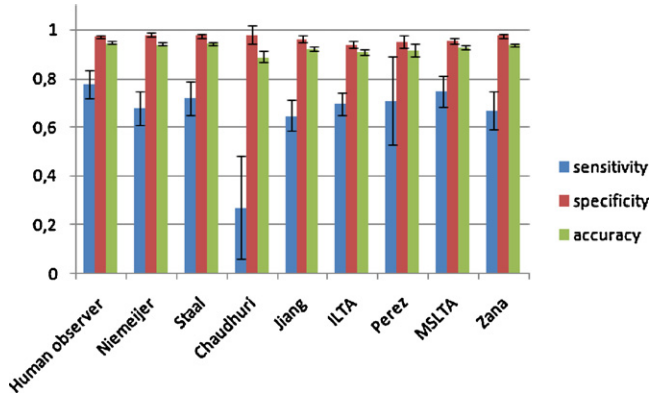

Fig. 11. Average sensitivity, specificity and accuracy for the vessel segmentation methods presented in Table 2.

Initially, two different implementations of the *MSLTA* using different estimators of V_1 are evaluated. Table 1 shows the mean sensitivity, specificity and accuracy of the *MSLTA* obtained using the similar but not identical Eqs. (4) and (5).

The two different *MSLTA* implementations are evaluated in terms of computational efficiency by comparing the average run-times for each *MATLAB R2008b* implementation. The run-times ratio $t(4)/t(5)$ of the mean estimation time for the cross-sectional profile parameter V_1, using the two equations as described in step "4. *Estimation of a new line-tracking pixel*" is 2.187, improving the computational efficiency by a factor of two.

In Fig. 9, the ROC curves obtained for various values of T_c are shown. Both curves show excellent behavior and in most cases the approximation of Eq. (5) outperforms the ROC curve derived by the standard estimation Eq. (4). Moreover, the ROC differences between the two implementations are insignificant, giving slightly better segmentation accuracy for the approximation of Eq. (5) compared to the standard estimator of Eq. (4) and in less than half-time.

In Fig. 10, the mean sensitivity, specificity and accuracy of the *MSLTA* using different estimations of the cross-sectional profile parameter V_1 and different processing modules are shown. It is evident that each module increases the accuracy and the specificity of the algorithm in both cases.

In Table 2, a comparison of the *MSLTA* using Eq. (4) with the most popular algorithms [3,4,14,22,28–30] is presented, while Fig. 11 shows a graphical representation of the results. More specifically, the *Human Observer* in this table shows the sensitivity, the specificity and the accuracy using the manual segmentation data

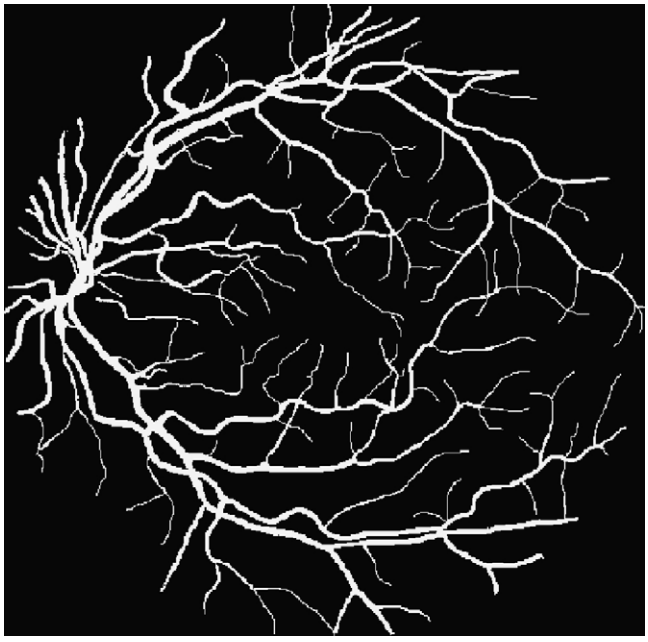

Fig. 12. Manual segmentation of the first observer for the first image of the *DRIVE* database.

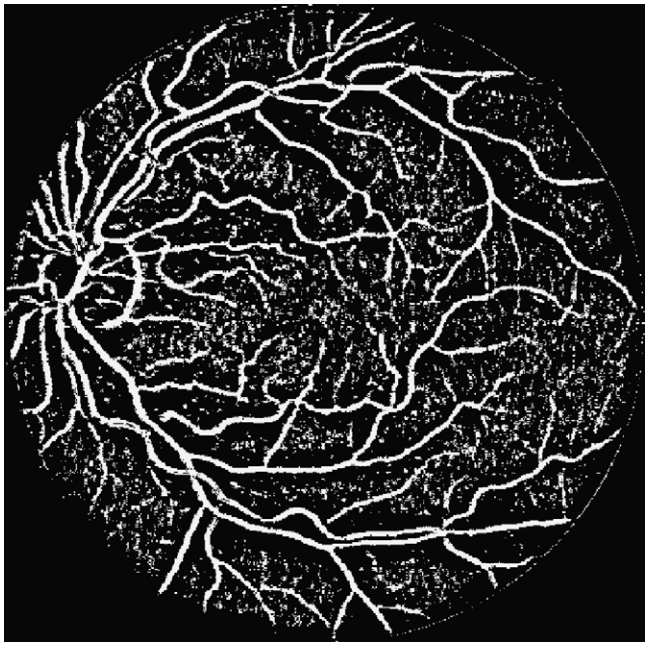

Fig. 13. Initial vessel map obtained using local neighborhood thresholding using the *ILTA*.

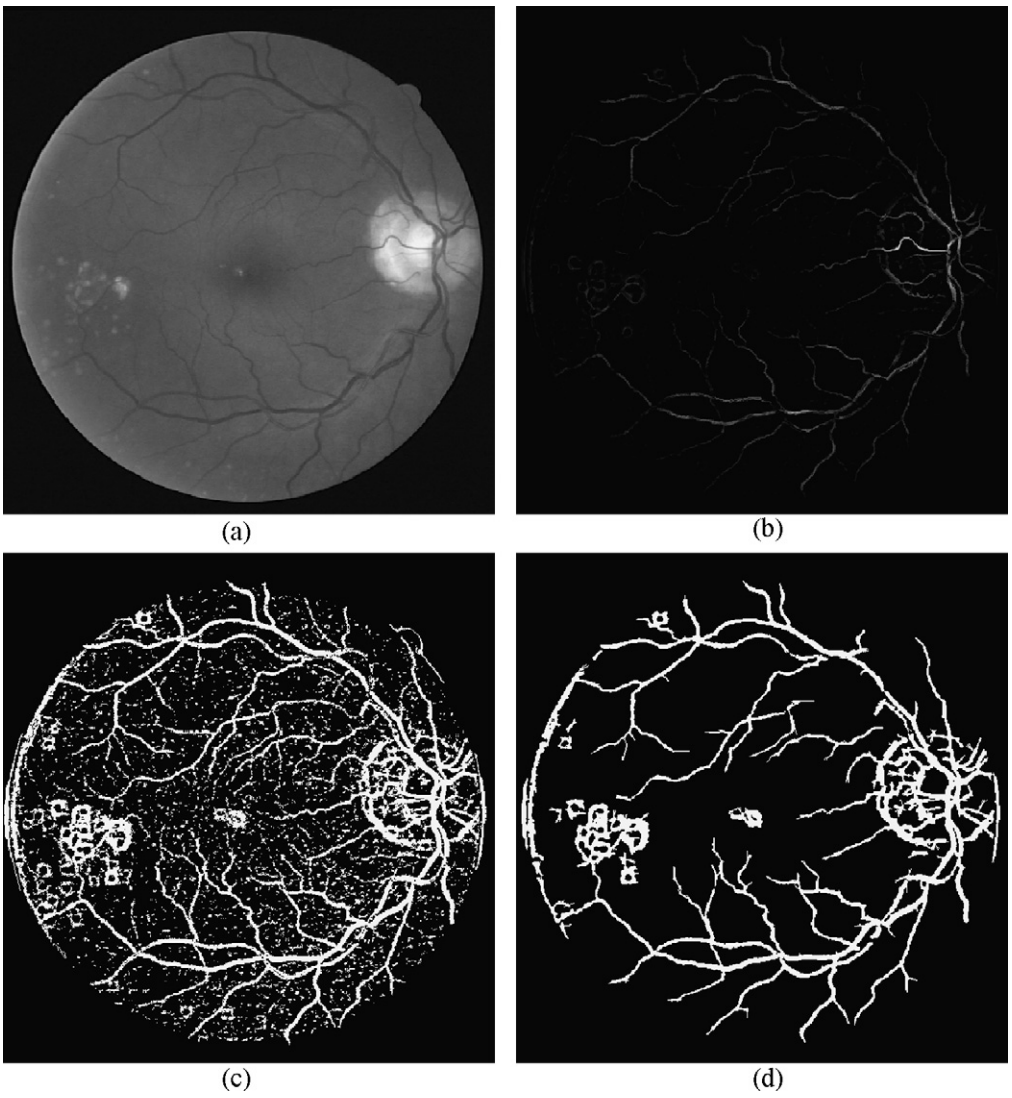

Fig. 14. (a) Original pathological image (08_test.tif), (b) confidence array, (c) map quantization, (d) morphological reconstruction.

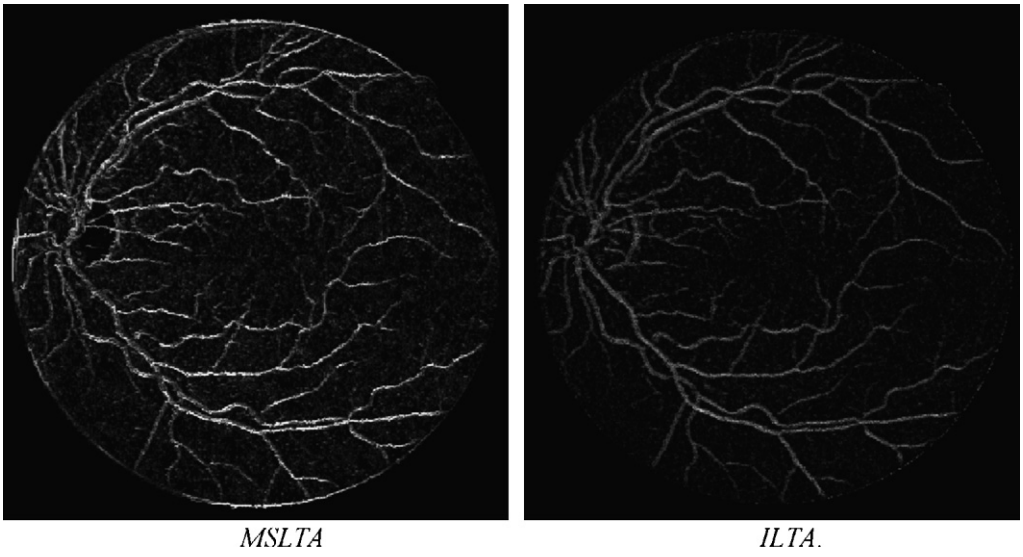

Fig. 15. Confidence array for the first image distorted by Salt&Pepper noise (density 0.05).

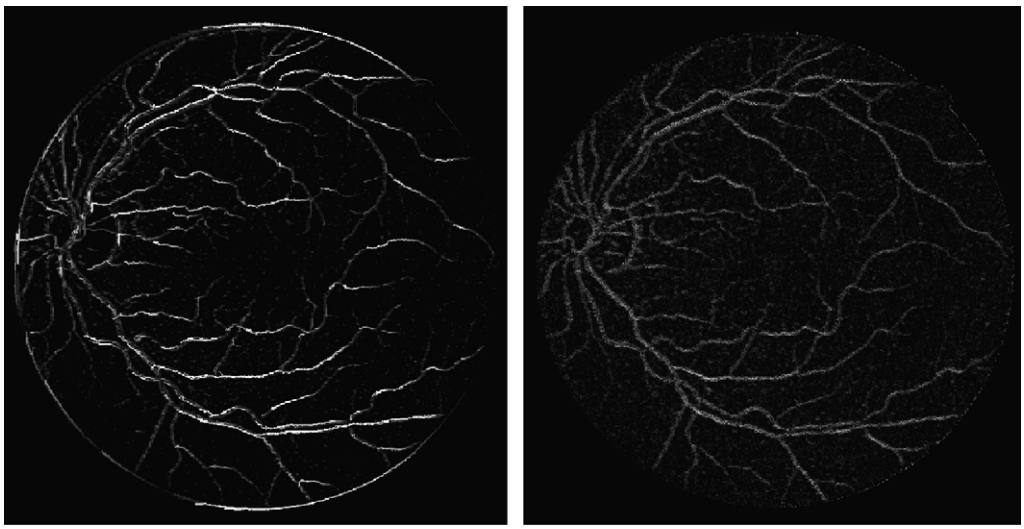

Fig. 16. Confidence array for the first image distorted by Salt&Pepper noise (density 0.1).

obtained from the second observer. The remaining lines present the same measures obtained from the compared methods including also the proposed *MSLTA*. The experimental results of the compared methods have already been published in the website of the *DRIVE* project [23].

In the first study Chaudhuri et al. [4] blood vessels in retinal images are detected using two-dimensional matched filters. The grey level cross-sectional profile of a blood vessel is approximated by a Gaussian shaped curve, detecting piecewise linear segments of blood vessels. The experimental results of this method, in terms of the measures used for evaluation, are poor when compared to other methods and the manual segmentation of the second observer. Furthermore, the method requires a large number of convolutions with large kernels in different directions in order to detect the retinal vasculature and also multi-scale information was not exploited.

The second study of Jiang and Mojon [29] presents a general framework of adaptive local thresholding, based on a multi-threshold probing scheme. Object hypotheses are generated by binarization using hypothetic thresholds and a verification procedure is used to accept these objects. This approach presents lower average sensitivity than the *MSLTA* in similar accuracy and specificity. However, the sensitivity of this method can be manipulated by changing the parameters of the verification procedure.

In contrast to the two previous unsupervised studies, the experimental results of a supervised approach are given in Niemeijer et al. It is a simple vessel segmentation method based on pixel classification [28]. For each pixel a feature vector is constructed and a *KNN* classifier is trained with these features vectors. In the last processing module, a *KNN* classifier is applied using a feature vector of 31 elements (Gaussian and its derivatives up to second order and at scales 1, 2, 4, 8, 16 and the original green channel's intensity). Although this method is supervised has lower sensitivity comparing with the *MSLTA*. The accuracy of this study is comparable with that of the second observer.

The fourth study of Perez et al. [30] presents a method for retinal blood vessel segmentation based upon the scale-space analysis of the first and second derivative of the brightness, which gives information about its topology and overcomes the problem of contrast variations. The local maxima of the magnitude gradient over scales and the maximum principal curvature are used as the two features in a two-stage region growing procedure. The

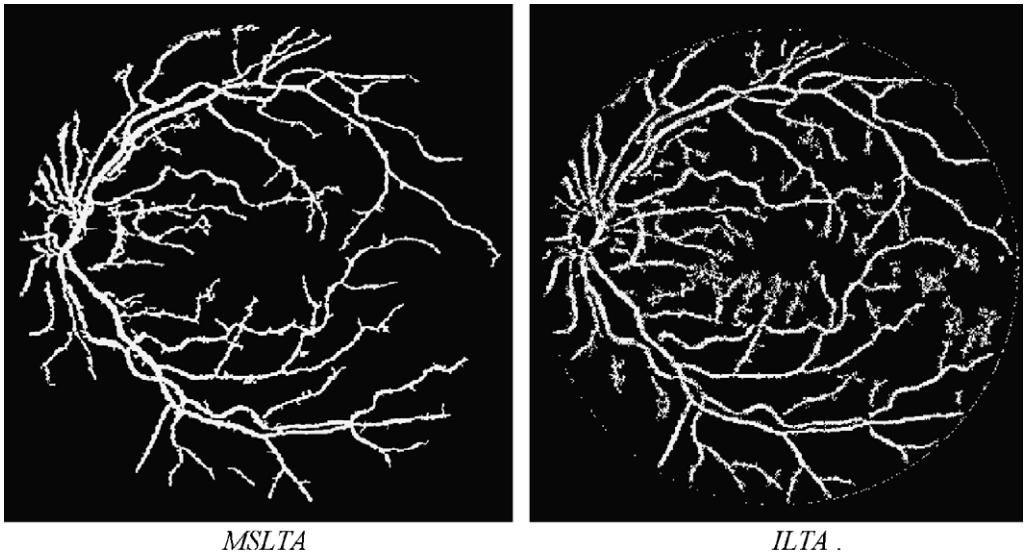

Fig. 17. Vessel map of the first image distorted by Salt&Pepper noise (density 0.05).

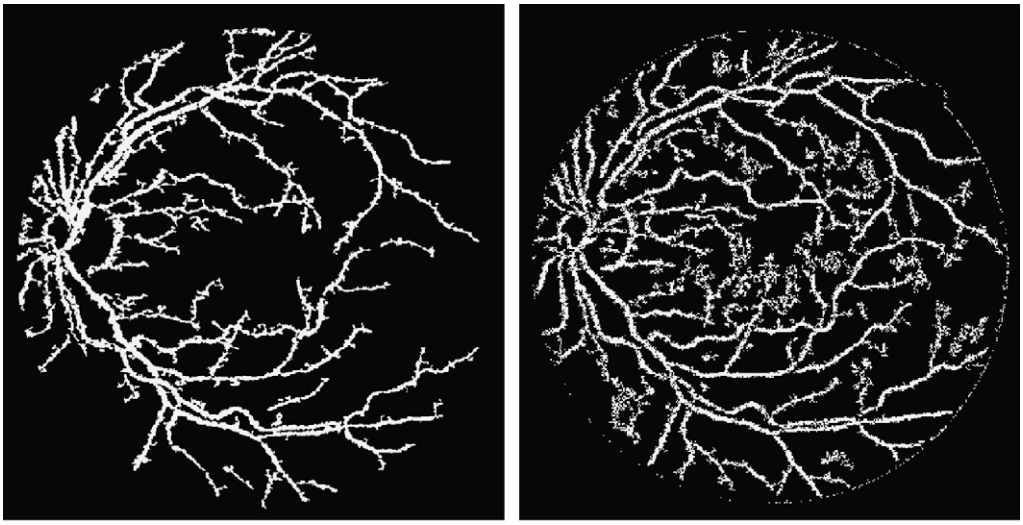

Fig. 18. Vessel map of the first image distorted by Salt&Pepper noise (density 0.1).

proposed *MSLTA* outperforms the fourth algorithm in all three measures.

In Staal et al. [3] the experimental results for automated segmentation of vessels in retinal images is based on image ridges extraction, which coincide approximately with vessel centerlines are presented. The ridges are used to compose primitives in the form of line elements. This information is used for partitioning the original image into patches by assigning each image pixel to the closest line element. Every line element constitutes a local coordinate frame for its corresponding patch. At each pixel, feature vectors are estimated that make use of patch properties and the line elements data. The feature vectors are classified using a nearest neighbor classifier. A relatively high rate of accuracy was achieved by this supervised method, comparable with the segmentation accuracy of the second observer, but lower sensitivity and slightly higher specificity than the *MSLTA* is measured.

The Zana and Klein [14] presents the experimental results of an algorithm based on mathematical morphology and curvature evaluation for the detection of vessel-like patterns in a noisy environment. The vessels are assumed to be a set of piece-wise locally linear connected elements, a hypothesis well formulated by mathematical morphology methods but also other tissue structures and spatial noisy patterns fit such description. In order to differentiate vessels from similar background patterns, a cross-curvature evaluation is performed. This algorithm has higher accuracy and lower sensitivity than the *MSLTA* in the same range of specificity.

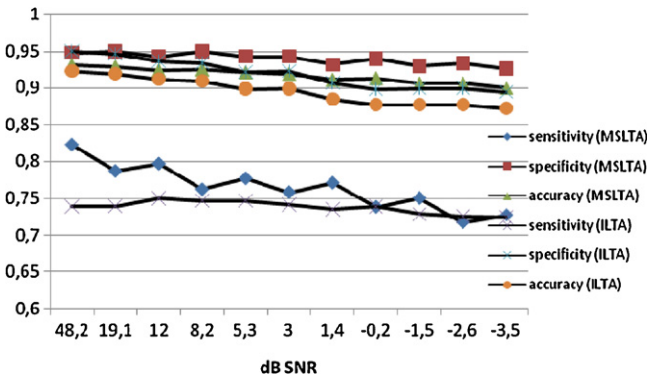

Fig. 19. Sensitivity, specificity and accuracy for the first image of the *DRIVE* database distorted by Salt&Pepper noise for both *MSLTA* and *ILTA*.

The evaluation and comparison between the iterative line-tracking algorithm [22] and the *MSLTA* is performed with respect to the first observer's segmentation (Fig. 12). In the *ILTA*, several manually defined parameters are required. In order to perform a fair comparison with the *MSLTA*, the number of repetitions for the *ILTA* was set to five million. The parameter W that represents the width of the cross-sectional profile was set to 11, which corresponds to the larger vessel's diameter. The distance r between the current tracking pixel and the testing cross-section was set to 1. The parameters p_{lr}, p_{ud} were set to 0.33, because vessels originated from the optic disk and various directions. The adopted parameters permit all vessels directions with the same probability. The threshold T, which is used to recognize vessel structures from the curvature of the cross-sectional profile was set to 10. Finally, a window neighborhood of size 31×31 is adopted for the binarization of confidence array by local neighborhood thresholding.

In the *MSLTA*, the parameter W was set to 3, 5, 7, 9 and 11, describing the expected range of vessel's diameter in pixels. The distance r between the current tracking pixel and the testing cross-section, was set to 1. In all cases, the eight pixel neighborhood was used and the parameter T was set to 10. In the map quantization process the hard threshold of five scales was adequate to indicate the presence of a vessel pixel. Outliers that may have remained from this quantization process are further removed using the morphological post-processing step. In both algorithms, a line structuring element of 13 pixels length ($M = 13$) is used for morphological directional filtering, and a disk structuring element with radius of 2 pixels ($R = 2$) is implemented for morphological reconstruction.

In Figs. 5–7 and 13, the intermediate images produced at different processing steps of both algorithms using the described parameter settings in the first image of the *DRIVE* database are shown. Fig. 5c shows the confidence array obtained from the *ILTA*, while Fig. 5a shows the multi-scale confidence array produced by the *MSLTA*. Figs. 13 and 6 show the binary images produced by local neighborhood thresholding and the map quantization process respectively for the two algorithms.

In Fig. 5d and b the extracted vessel network obtained from *ILTA* and *MSLTA* are shown. From these two images and the quantitative results presented in Table 2, it is evident that the *MSLTA* outperforms the *ILTA* in terms of sensitivity, specificity and accuracy in the images of the *DRIVE* database.

In Fig. 14, a typical pathological retinal image is shown. The proposed *MSLTA* enhances all region-of-interest, i.e. both ves-

sel network and pathological findings. This effect is desired in computer-aided diagnosis tools.

As shown in Fig. 14d, there are detectable false positives on the boundary of the images. These false positives are presented in the segmented images due to the fact that the cross-section of the boundary has similar shape with the vessels' profile. Thus, if pixels very close to the boundary are automatically selected by the seed extraction procedure, it is inevitable that a small part of the boundary would be tracked. These false positives can be removed by a supervised algorithm, if the information given by the provided mask is exploited. This capability is not available in the unsupervised *MSLTA*.

Additional experiments are conducted to evaluate the *ILTA* and *MSLTA* robustness in terms of segmentation sensitivity, specificity and accuracy in the presence of Gaussian and Salt&Pepper noise. Assuming an almost noise-free *DRIVE* database, additive noise is used to distort the *DRIVE* images using ten different levels of noise. In the experiments conducted with low level additive noise, the methods' robustness in noise levels met in medical devices is studied. On the contrary, in the experiments where the unrealistic high level of noise is present, the weakest processing modules of *MSLTA* are detected. The original image, assuming free of noise, with brightness values in the range between 0 and 1 was distorted by additive Salt&Pepper noise with density 0.05 and 0.1. In Figs. 15 and 17 the confidence arrays produced by processing the noisy images for both *MSLTA* and *ILTA* are shown. In Figs. 16 and 18 the corresponding vessel maps for both algorithms and levels of noise are shown. In Figs. 19 and 20 the experimental results of the *MSLTA* and *ILTA* in noise are presented in terms of sensitivity, specificity and accuracy. As the results shown, the proposed algorithm is robust against noise even in case of low *SNRs* and met the segmentation accuracy of the *ILTA* derived from the undistorted original images. In the case where the original image has distorted by Salt&Pepper noise with density 0.05, the proposed algorithm presents slightly higher sensitivity and slightly lower specificity in the same accuracy with *ILTA*. In lower *SNRs* the proposed algorithm presents a gradual decrease in terms of accuracy, as expected.

In Fig. 19, the sensitivity, specificity and accuracy of the *MSLTA* and the *ILTA* of the first image of the *DRIVE* database, artificially distorted using Salt&Pepper noise in various levels of noise between 45 and −5 dB *SNR* is shown. The proposed algorithm is extremely robust in this type of noise, slightly decreasing in specificity and accuracy rates as the noise level increases. The non-monotonic

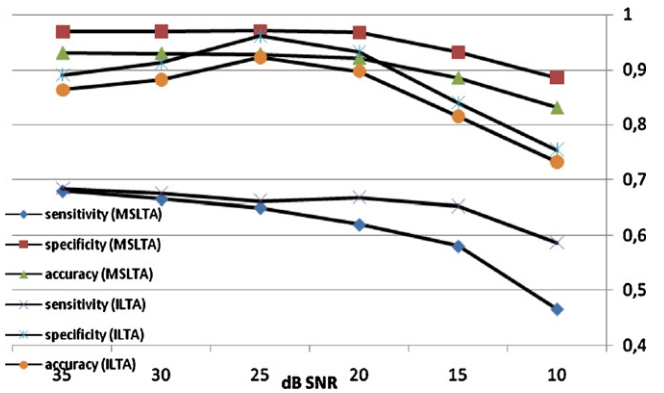

Fig. 20. Sensitivity, specificity and accuracy for the first image of the *DRIVE* database distorted by additive Gaussian noise in dB *SNR* for both *MSLTA* and *ILTA*.

shape of the sensitivity curve in Fig. 19 suggests that it is possible to get better results by adding Salt&Pepper noise. In few occasions, this type of noise improves the vessel network continuity, producing better sensitivity rates. Almost the same conclusions have been extracted for *ILTA*.

In Fig. 21, the confidence arrays of the *MSLTA* and *ILTA* are shown when the original image is distorted by Gaussian noise with zero mean value and variance equal to 0.005. In Fig. 22, the extracted vessel maps are given. The experimental results of Figs. 20–22, shown that the robustness of both algorithms in case of additive Gaussian noise is significantly less effective. The most important source of this weakness is due to the Gaussian-like shape of the cross-sectional profile. The artificial additive noise produces a great number of faulty Gaussian-like cross-sectional profiles.

Alternatively, instead of the morphological post-processing described in steps 8 and 9, a similar procedure called length filtering can be employed to eliminate the image misclassifications. According to length filtering, the procedure of noise elimination is implemented as follows: A region of connected pixels is estimated from the vessel map after median filtering using the rule of eight-pixel connectivity. All regions with size less than an experimentally derived threshold, are eliminated. The remaining regions, surviving after length filtering, constitute the final vessel network. Although both post-processing approaches produce similar results, as shown in Table 3, in this work the morphological post-processing of steps

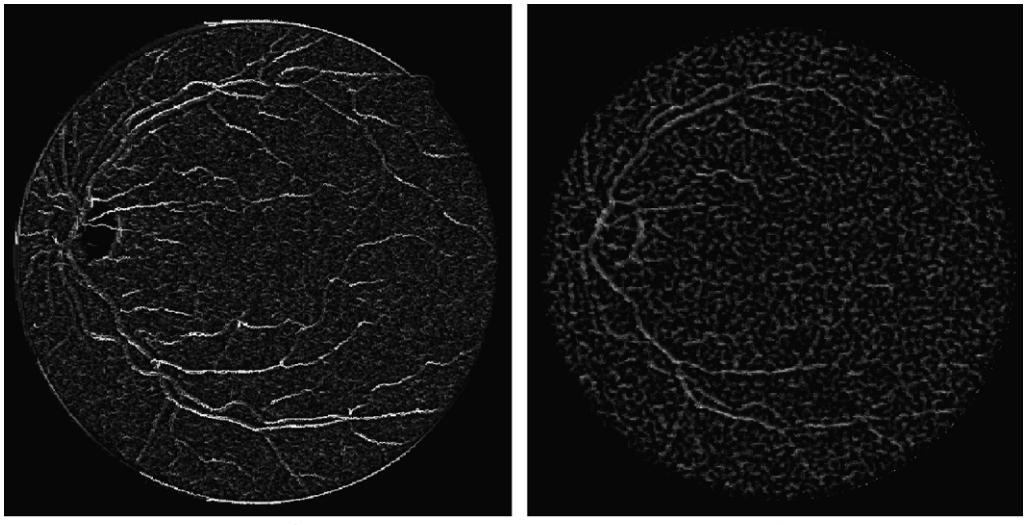

Fig. 21. Confidence array for the first image distorted by Gaussian noise with zero mean value and variance equal to 0.005.

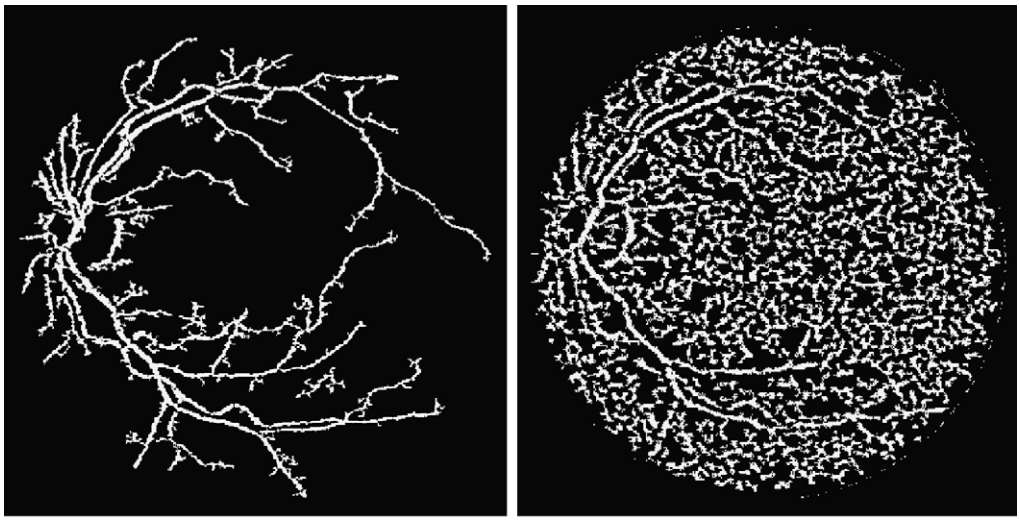

Fig. 22. Vessel map of the first image distorted by Gaussian noise with zero mean value and variance equal to 0.005.

Table 3
Comparison between morphological post-processing and length filtering in terms of accuracy, sensitivity and specificity in *MSLTA*.

	Length filtering			Morphological post-processing		
	Sensitivity	Specificity	Accuracy	Sensitivity	Specificity	Accuracy
Average	0.7602	0.9490	0.9249	0.7468	0.9551	0.9285
Standard deviation	0.0626	0.0145	0.0105	0.0654	0.0128	0.0088

8 and 9 is adopted to obtain a fair comparison between *ILTA* and *MSLTA*.

5. Conclusions

In this paper an algorithm for multi-scale retinal vessel segmentation is proposed. The algorithm is based on a novel seeded multi-scale line-tracking procedure and morphological post-processing. A fast tracking process starts the estimation of a confidence matrix from a group of seeds, extracted from image's histogram, and continues until a specific condition of the cross-sectional profile becomes invalid. The intermediate multi-scale image map arises after processing the individual image maps along scales and contains an estimation of each pixel confidence to belong in a vessel. The initial vessel network is derived after map quantization. In the sequel, median filtering is applied in the initial vessel network in order to restore disconnected vessel lines or to eliminate noisy lines. Although the produced network in most cases is acceptable, post-processing methods remove efficiently erroneous areas using directional attributes of vessels and morphological reconstruction. The experimental evaluation of the proposed method in the *DRIVE* database shows robust extraction of vessels network. The average accuracy of the proposed algorithm is 0.929 with 0.747 sensitivity and 0.955 specificity, which is near to the manual segmentation of the second observer. The *MSLTA* gives the higher average sensitivity among all compared supervised and unsupervised methods in almost the same specificity rate. Additional experiments carried out using the testing set of the *DRIVE* database shown superior sensitivity, specificity and accuracy for the proposed method compared to the rates obtained by *ILTA*. Moreover, the proposed algorithm is tested under noise presence and it proved that it is robust in additive Salt&Pepper noise even in case of low *SNRs*, having almost the same behavior as *ILTA* applied to the undistorted images. The major drawback of the proposed algorithm, which is also a drawback of the *ILTA*, is the high misclassification rate of the optic disk.

Acknowledgement

This work was supported in part by University of Patras, under Grant Karatheodoris.

References

[1] Leandro JJG, Cesar Jr RM, Jelinek H. Blood vessels segmentation in retina: preliminary assessment of the mathematical morphology and of the wavelet transform techniques. In: Proceedings of the 14th Brazilian symposium on computer graphics and image processing. 2001. p. 84–90.
[2] Soares JVB, Leandro JJG, Cesar Jr RM, Jelinek HF, Cree MJ. Retinal vessel segmentation using the 2D Morlet wavelet and supervised classification. IEEE Trans Med Imaging 2006;25(9):1214–22.
[3] Staal J, Abramoff MD, Niemeijer M, Viergever MA, van Ginneken B. Ridge-based vessel segmentation in color images for the retina. IEEE Trans Med Imaging 2004;23(4):501–9.
[4] Chaudhuri S, Chatterjee S, Katz N, Nelson M, Goldbaum M. Detection of blood vessels in retinal images using two-dimensional matched filters. IEEE Trans Med Imaging 1989;8(3):263–9.
[5] Chutatape O, Zheng L, Krishnan SM. Retinal blood vessel detection and tracking by matched Gaussian and Kalman filters. In: Proceedings of the 20th annual international conference of the IEEE on engineering in medicine and biology, vol. 6. 1998. p. 3144–9.
[6] Chanwimaluang T, Guoliang F. An efficient blood vessel detection algorithm for retinal images using local entropy thresholding. Proc Int Symp Circuits Syst (ISCAS) 2003;5:21–4.
[7] Li H, Chutatape O. Automated feature extraction in color retinal images by a model based approach. IEEE Trans Biomed Eng 2004;51(2):246–54.
[8] Walter T, Kein JC, Massin P, Erginay A. A contribution of image processing to the diagnosis of diabetic retinopathy—detection of exudates in color fundus images of the human retina. IEEE Trans Med Imaging 2002;21(10):1236–43.
[9] Kondo T. Detection of anatomical features in retinal images using gradient orientation. In: IEEE TENCON. 2004.
[10] Pajak R. Use of two-dimensional matched filters for estimating a length of blood vessels newly created in angiogenesis process. Opt Electron Rev 2003;11(3):237–41.

[11] Hoover AD, Kouznetsova V, Goldbaum M. Locating blood vessels in retinal images by piecewise thresholdprobing of a matched filter response. IEEE Trans Med Imaging 2000;19:203–10.
[12] Can A, Shen H, Turner JN, Tanenbaum HL, Roysam B. Rapid automated tracing and feature extraction from retinal fundus images using direct exploratory algorithms. IEEE Trans Inform Technol Biomed 1999;3(2):125–38.
[13] Goldbaum M, Moezzi S, Taylor A, Chatterjee S, Boyd J, Hunter E, et al. Automated diagnosis and image understanding with object extraction, object classification and inferencing in retinal images. La Jolla, California 92093-0946, USA: Department of Ophthalmology and Department of Engineering and Computer Science, University of California. 1996.
[14] Zana F, Klein J-C. Segmentation of vessel-like patterns using mathematical morphology and curvature evaluation. IEEE Trans Image Process 2001;10:1010–9.
[15] Bevilacqua V, Cambò S, Cariello L, Mastronardi G. A combined method to detect retinal fundus features. In: European conference on emergent aspects in clinical data analysis EACDA. 2005.
[16] Gang L, Chutatape O, Krishnan SM. Detection and measurement of retinal vessels in fundus images using amplitude modified second-order Gaussian filter. IEEE Trans Biomed Eng 2002;49(2):168–72.
[17] Mohamed C, Auda G. An algorithm for enhancing retinal vessel detection filters. Med Image Understand Anal 2002.
[18] Condurache AP, Aach T, Eck K, Bredno J, Grzybowsky S, Machens HG. Vessel segmentation for angiographic enhancement and analysis, in: Bildverarbeitung für die Medizin 2005 (Algorithmen Systeme Anwendungen). Heidelberg; 2005. p. 173–177.
[19] Sofka M, Stewart CV. Retinal vessel centerline extraction using multiscale matched filters. Confidence and edge measures. IEEE Trans Med Imaging 2006;25:1531–46.
[20] Miura N, Nagasaka A, Miyatake T. Feature extraction of finger-vein patterns based on iterative line tracking and its application to personal identification. Syst Comput Jpn 2004;35(7):61–71.
[21] Miura N, Nagasaka A, Miyatake T. Feature extraction of finger-vein patterns based on repeated line tracking and its application to personal identification. Mach Vision Appl 2004;15:194–203.
[22] Vlachos M, Dermatas E. Vessel network extraction in retinal images using iterative line tracking. In: 8th international workshop on mathematical methods in scattering theory and biomedical engineering. 2007.
[23] http://www.isi.uu.nl/Research/Databases.
[24] Foracchia M, Grisan E, Ruggeri A. Luminosity and contrast normalization in retinal images. Med Image Anal 2005;9:179–90.
[25] Gongalez RC, Woods RE, Eddins SL. Digital image processing using MATLAB. Prentice Hall; 2004.
[26] Vincent L. Morphological grayscale reconstruction in image analysis: applications and efficient algorithms. IEEE Trans Pattern Anal Mach Intell 1993;13(6):583–98.
[27] Foracchia M, Grisan E, Ruggeri A. Detection of optic disc in retinal images by means of a geometrical model of vessel structure. IEEE Trans Med Imaging 2004;23:1189–95.
[28] Niemeijer M, Staal J, van Ginneken B, Loog M, Abramoff MD. Comparative study of retinal vessel segmentation methods on a new publicly available database. Proc SPIE Med Imaging 2004;5370:648–56.
[29] Jiang X, Mojon D. Adaptive local thresholding by verification-based multithreshold probing with application to vessel detection in retinal images. IEEE Trans Pattern Anal Mach Intell 2003;25(1):131–7.
[30] Perez M, Hughes A, Stamton A, Thom S, Bharath A, Parker K. Retinal blood vessel segmentation by means of scale-space analysis and region growing. In: Proceedings of the medical image computing and computer-assisted intervention-MICCAI'99, vol. 1679/1999. 1999. p. 90–7.

Marios Vlachos was born in Sparti, Greece, in 1981. He received his diploma in Electrical Engineering and Computer Technology from University of Patras, Greece, in 2004. Since 2004, he has been with department of Electrical Engineering and Computer Technology of University of Patras where he is a PhD candidate. His research interests focus on biomedical image processing and analysis, pattern recognition and biometrics.

Evangelos Dermatas is Associate Professor at the Department of Electrical and Computer Engineering of the University of Patras, Patras, Hellas. He received his Diploma and PhD degrees from the Department of Electrical Engineering of the University of Patras, Patras, Hellas in 1985 and 1991 respectively. His research interest areas include: medical imaging, Speech & natural language processing, statistical signal processing, pattern recognition.